Composites: Part A 48 (2013) 47–56

Contents lists available at SciVerse ScienceDirect

Composites: Part A

journal homepage: www.elsevier.com/locate/compositesa

A matricial approach of fibre breakage in twin-screw extrusion of glass fibres reinforced thermoplastics

Audrey Durin [a], Pascal De Micheli [a], Julien Ville [b,c], Funda Inceoglu [d], Rudy Valette [a], Bruno Vergnes [a,*]

[a] MINES ParisTech, Centre de Mise en Forme des Matériaux (CEMEF), UMR CNRS 7635, BP 207, 06904 Sophia Antipolis, France
[b] POLYTECHS SA, 76 450 Cany-Barville, France
[c] Laboratoire d'Ingénierie des Matériaux de Bretagne, EA 4250, Université de Bretagne Occidentale, 29 238 Brest, France
[d] ARKEMA, CERDATO, 27 470 Serquigny, France

ARTICLE INFO

Article history:
Received 29 February 2012
Received in revised form 20 December 2012
Accepted 31 December 2012
Available online 19 January 2013

Keywords:
A. Glass fibres
C. Micro-mechanics
C. Computational modelling
E. Extrusion

ABSTRACT

Limiting fibre breakage during composite processing is a crucial issue. The purpose of this paper is to predict the evolution of the fibre-length distribution along a twin-screw extruder. This approach relies on using a fragmentation matrix to describe changes in the fibre-length distribution. The flow parameters in the screw elements are obtained using the simulation software Ludovic®. Evolution of an initial fibre-length distribution for several processing conditions was computed and the results were compared with experimental values. The computation gives satisfying results, even though more comparisons with experiments would be necessary.

1. Introduction

A classical use for glass fibres in industry is thermoplastic polymers reinforcement, mostly for injected parts. Long-fibre composites are known to offer better mechanical properties than short-fibre ones. Consequently, an important point is to preserve as much as possible long fibres during compounding, despite strong flow conditions, eventually leading to severe break-up.

Fibre orientation for long-fibre thermoplastics in moulding process has already been studied and modelled [1–4] and a quantitative model predicting changes in fibre-length distribution during mould filling has been recently developed by Tucker et al. [5]. However, prior to injection moulding, other processes are used to compound glass fibres into polymer matrices. An important issue is thus to control fibre lengths in these processes to subsequently inject compounds exhibiting a suitable final length distribution. The most common of these processes is twin-screw extrusion, in which considerable fibre length degradation occurs [6–8]. Shon et al. [9] have been the firsts to develop an empirical model describing the average fibre length evolution in different continuous processes, including twin-screw extrusion. More recently, this approach was improved to calculate average fibre length evolution during twin screw extrusion and Buss kneader compounding [10–11]. However, these methods do not provide information on the whole fibre-length distribution. Therefore, the aim of the present paper is to propose a computational method to predict changes in the fibre-length distribution along a twin-screw extruder.

2. Theoretical model

2.1. Forgacs and Mason model

Our model is based on the assumption that fibre breakage is only due to flow-induced buckling, as described by Forgacs and Mason [12]. According to this model, a rotating rigid fibre in a shear flow may break when oriented in the direction of compressive forces. Beyond a critical force, which depends on its mechanical properties and length, the fibre buckles and then breaks-up (Fig. 1). Breakage occurs because of the severe tensile stress σ_s induced on the external surface of the fibre when it is bending. This stress depends on the fibre radius b, its Young modulus E and the local radius of curvature R:

$$\sigma_s(x) = -\frac{Eb}{R(x)} \tag{1}$$

where x is the abscissa along the fibre principal axis. When the stress σ_s on the surface reaches the tensile strength value of the fibre σ_c, the fibre breaks-up. As the radius of curvature of the fibre is linked to the fibre deformation, the breakage phenomenon directly depends on this deformation. In this work, it was assumed that, when buckling occurs, the fibre systematically breaks-up because

* Corresponding author. Tel.: +33 493 957 463; fax: +33 492 389 752.
E-mail address: bruno.vergnes@mines-paristech.fr (B. Vergnes).

1359-835X/$ - see front matter © 2013 Elsevier Ltd. All rights reserved.
http://dx.doi.org/10.1016/j.compositesa.2012.12.011

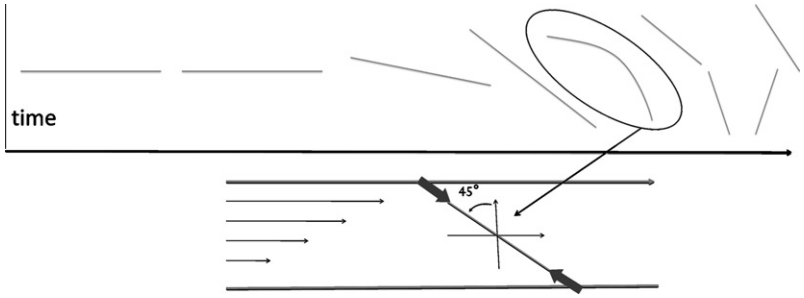

Fig. 1. Rotating fibre in a shear flow. Break-up occurs when the maximum flow-induced compressive force is high enough.

of the resulting huge deformation. This assumption is validated in Section 2.3.

2.2. Jeffery equation

To determine when buckling (and then breakage) occurs, forces applied on the fibre as well as fibre orientation must be computed. Classically, the orientation **P** of a single ellipsoidal fibre of length $2a$ and radius b in a shear flow is obtained by solving Jeffery equation [13]:

$$\dot{\mathbf{P}} = \boldsymbol{\Omega} \cdot \mathbf{P} + \lambda[\dot{\boldsymbol{\varepsilon}} : \mathbf{P} - (\dot{\boldsymbol{\varepsilon}} : \mathbf{P} \otimes \mathbf{P})\mathbf{P}] \tag{2}$$

where **P** is the orientation vector of the fibre principal axis, $\boldsymbol{\Omega}$ the vorticity tensor, $\dot{\boldsymbol{\varepsilon}}$ the strain rate tensor, and λ a parameter related to the aspect ratio $\beta = a/b$:

$$\lambda = \frac{\beta^2 - 1}{\beta^2} \tag{3}$$

The orientation vector **P** describes the fibre orientation in the reference frame. In the case of simple shear flow, this frame is defined as depicted in Fig. 2. This orientation can also be described by the angles θ and ϕ (which can be determined from **P**). As glass fibres are cylindrical, the ellipsoid aspect ratio β should be replaced in Eq. (3) with an equivalent aspect ratio β_e for cylinders, theoretically determined by Burgers [14]:

$$\beta_e = 0.74\beta \tag{4}$$

The orientation vector was then used in the forces computation. The shear induced force F_B, integrated on a half-fibre, was given by Burgers [14], without further indication on the forces distribution f along the fibre:

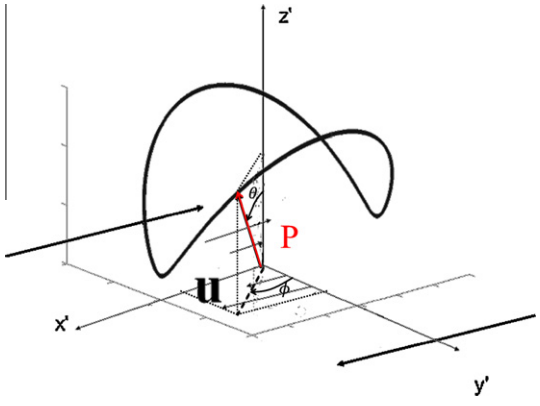

Fig. 2. Fibre end orbit in a simple shear flow. The shear plan frame (x', y', z') is translating with the fibre. (For interpretation of the references to colour in this figure legend, the reader is referred to the web version of this article.)

$$F_B = -\int_a^0 f(x)\, dx = \frac{M\pi\eta\dot{\gamma}a^2}{\ln(2\beta) - 1.75} \tag{5}$$

where η is the viscosity and $\dot{\gamma}$ the shear rate. M is defined as:

$$M = \sin^2\theta \sin\phi \cos\phi \tag{6}$$

where θ and ϕ were obtained from the orientation vector **P**. In a more convenient form, Eq. (5) can be written in terms of stress:

$$\sigma_B = \eta\dot{\gamma}M\frac{\beta^2}{\ln(2\beta) - 1.75} \tag{7}$$

In order to determine when buckling occurred, forces were assumed to be punctually applied at fibre ends. Then, it was possible to obtain the buckling threshold by applying Euler buckling method.

2.3. Euler buckling method

In order to confirm that perfect (without any defect) rigid fibres cannot break-up when simply bending below the buckling threshold (in the case of small deformations) and also always break-up when buckling, the tensile stress σ_s applied on the external surface of the fibre when it bends (below the buckling threshold: small deformation) and when it buckles (over the buckling threshold: large deformation) must be computed. In this way, the tensile stress σ_s can be compared to the tensile strength σ_c in order to check if the fibre does break. Compressive forces were supposed to be only applied at fibre ends and along its principal direction. The bending momentum balance for a non-deformed configuration gives:

$$M_0(x) = F_B y(x) \tag{8}$$

where $M_0(x)$ is the bending momentum and $y(x)$ the fibre deflection at point x. From this equation, the deformation below the buckling threshold (assuming that there exists an initial deflection at rest) and beyond the buckling threshold can be obtained. First, the buckling threshold was calculated under the assumption of "small" deformations (Euler buckling method), in which the bending momentum M_0 is approximated by:

$$M_0 = \frac{EI}{R} \approx EIy'' \tag{9}$$

where I is the moment of inertia and R the radius of curvature. Combining Eqs. (8) and (9) leads to the differential equation:

$$y'' + k^2 y = 0 \tag{10}$$

with $k^2 = -\frac{4}{b^2}\frac{\sigma_B}{E}$. The only possible non trivial solution satisfying the homogenous boundary conditions ($y(a) = 0$ and $y'(0) = 0$) is:

$$y = A\cos(kx) \tag{11}$$

with $k = p\frac{\pi}{2}a$ and p is a strictly positive integer. Considering that the fibre is brittle, and assuming that it breaks when it reaches its

first buckling mode ($p = 1$), leads to the expression of the maximal stress σ_m^e before buckling:

$$\sigma_m^e = -E\left(\frac{\pi}{4\beta}\right)^2 \tag{12}$$

Comparing the stress σ_B induced by the flow on the fibre with the maximal stress σ_m^e before buckling leads to a buckling parameter Bu:

$$Bu = \frac{\sigma_B}{\sigma_m^e} = -\left(\frac{4}{\pi}\right)^2 M\frac{\eta\dot{\gamma}}{E}\frac{\beta^4}{\ln(2\beta) - 1.75} \tag{13}$$

which is greater than 1 for a buckling fibre.

Below the buckling threshold, a perfectly straight fibre cannot be deformed applying only compressive forces. Fibres can however exhibit an initial deflexion as they are not ideal objects. In the framework of small deformations, below the first buckling mode, it is reasonable to consider an initial deflexion of the fibre of the form:

$$y_0 = h\cos\frac{\pi x}{2a} \tag{14}$$

where h is the arbitrary fixed initial deflexion for $x = 0$. Then, the deformation below the buckling threshold can be computed replacing y with $Y + y_0$ in Eq. (8) and y with Y in Eq. (9). The following differential equation was then obtained:

$$Y'' + k^2 Y = -k^2 h\cos\frac{\pi x}{2a} \tag{15}$$

The solution of this equation satisfying the boundary conditions is:

$$Y = h\frac{1}{1 - Bu}\cos\frac{\pi x}{2a} \tag{16}$$

From this expression and from Eq. (1), the expression of the local tensile stress $\sigma_s(x)$ applied on the external surface of the fibre below the buckling threshold was deduced under the hypothesis of small deformations ($\frac{1}{R} = Y''$):

$$\sigma_s(x) = E\frac{h}{b}\left(\frac{\pi}{2\beta}\right)^2\frac{1}{1 - Bu}\cos\frac{\pi x}{2a} \tag{17}$$

On the other hand, to calculate the deformation beyond the buckling threshold, the small deformations hypothesis can no longer be used. The deformation was then supposed large enough so that y' is no more negligible with respect to 1. Eq. (9) then becomes a non-linear second order differential equation:

$$M_0 = \frac{EI}{R} = EI\frac{y''}{(1 + y'^2)^{3/2}} \tag{18}$$

From Eqs. (8) and (18), the following non-linear differential equation was obtained:

$$\frac{y''}{(1 + y'^2)^{3/2}} + k^2 y = 0 \tag{19}$$

The solution of Eq. (19) with homogeneous boundary conditions is [15]:

$$y = a\frac{4\sqrt{2}}{\pi}\sqrt{Bu - 1}\left[1 - \frac{1}{8}(Bu - 1)\right]\cos\frac{\pi x}{2a} \tag{20}$$

From Eqs. (1) and (20), the expression of the local tensile stress $\sigma_s(x)$ applied on the external surface of the fibre over the buckling threshold was deduced:

$$\sigma_s(x) = E\frac{\frac{\pi\sqrt{2}}{\beta}\sqrt{Bu - 1}\left[1 - \frac{1}{8}(Bu - 1)\right]\cos\frac{\pi x}{2a}}{\left[1 + 8(Bu - 1)\left[1 - \frac{1}{8}(Bu - 1)\right]^2\sin^2\frac{\pi x}{2a}\right]^{\frac{3}{2}}} \tag{21}$$

Comparing these tensile stresses $\sigma_s(x)$ (Eqs. (17) and (21)) with the tensile strength σ_c of the fibre, a break-up parameter was obtained:

$$Br = \frac{\sigma_s(x)}{\sigma_c} \tag{22}$$

with

$$Br = \frac{E}{\sigma_c}\frac{h}{b}\left(\frac{\pi}{2\beta}\right)^2\frac{1}{1 - Bu}\cos\frac{\pi x}{2a} \quad \text{if } Bu < 1 \tag{23}$$

$$Br = \frac{E}{\sigma_c}\frac{\frac{\pi\sqrt{2}}{\beta}\sqrt{Bu - 1}\left[1 - \frac{1}{8}(Bu - 1)\right]\cos\frac{\pi x}{2a}}{\left[1 + 8(Bu - 1)\left[1 - \frac{1}{8}(Bu - 1)\right]^2\sin^2\frac{\pi x}{2a}\right]^{\frac{3}{2}}} \quad \text{if } Bu > 1 \tag{24}$$

Br depends on the buckling parameter $Bu = \frac{\sigma_B}{\sigma_m^e}$ and is greater than 1 for a theoretically perfect (i.e. without any defect) breaking fibre.

Some Bu and Br values will now be computed, for a range of parameter whose order of magnitude corresponds with the case of short glass fibres and polymer in a twin-screw extruder, in order to better understand the breakage phenomenon. These results are only illustrative and are not to be compared with the experimental results that are shown further. Fig. 3 shows the change of the breakage parameter Br as a function of the buckling parameter Bu for different values of relative shear stress $\frac{\eta\dot{\gamma}}{E}$ (from 2×10^{-8} to 3×10^{-6}) and aspect ratio β (from 10 to 200). Other parameters were kept constant: $x/a = 0$ (centre of the fibre), $h/b = 0.01$ (initial relative deflexion), $\phi = -\pi/4$, $\theta = \pi/2$ (fibre position in the flow), $E/\sigma_c = 30$ (fibre flexibility). In area (1), the fibre has not reached the buckling threshold nor the break-up threshold, so it remains straight and does not break. In area (2), only the break-up threshold is reached, so the fibre breaks-up instantaneously without buckling (weak fibre). In area (3), only the buckling threshold is reached, so the fibre buckles without breaking (flexible fibre). Finally, in area (4), both thresholds are reached, so the fibre breaks-up during buckling.

The effect of fibre orientation (angle θ) is shown in Fig. 4 for various aspect ratios β (from 10 to 600), the other parameters being constant: $x/a = 0$ (centre of the fibre), $h/b = 0.01$ (initial relative deflexion), $\phi = -\pi/4$ (fibre position in the flow), $\eta\dot{\gamma}/E = 10^{-7}$ (relative shear stress), $E/\sigma_c = 30$ (fibre flexibility). In the tested conditions, it was noticed that fibres were almost always breaking-up when buckling, justifying the proposed approximation that buckling is equivalent to break-up. It was thus possible to directly use

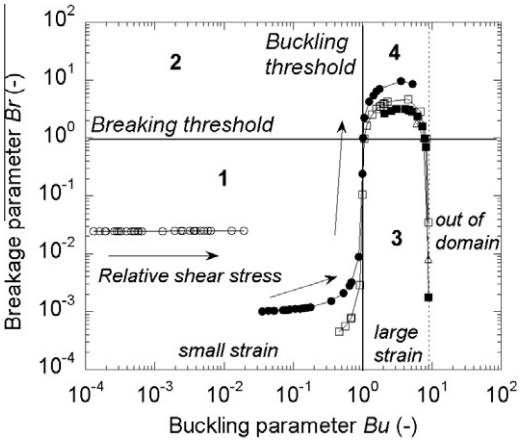

Fig. 3. Correlation between buckling parameter Bu and breakage parameter Br for different aspect ratios β. ○: $\beta = 10$; ●: $\beta = 50$; □: $\beta = 100$; ■: $\beta = 150$; △: $\beta = 200$ (the arrows indicate the evolution when changing the relative shear stress $\frac{\eta\dot{\gamma}}{E}$ from 2×10^{-8} to 300×10^{-8}, other parameters constant).

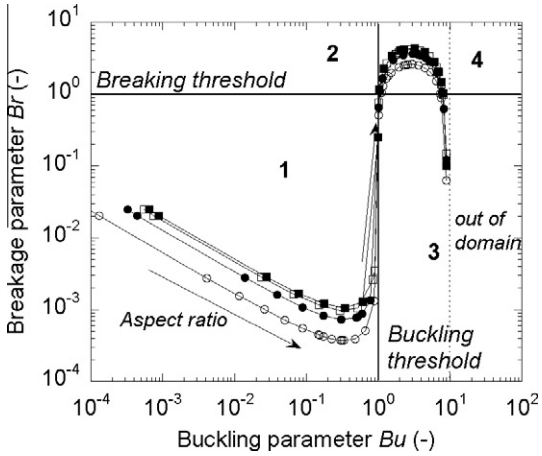

Fig. 4. Correlation between buckling parameter *Bu* and breakage parameter *Br* for different angles θ (with the z' axis perpendicular to the shear plan). ○: $\theta = \pi/8$; ●: $\theta = \pi/4$; □: $\theta = 3\pi/8$; ■: $\theta = \pi/2$ (the arrows indicate the evolution when changing the aspect ratio β from 10 to 600, other parameters constant).

the buckling parameter *Bu* (Eq. (10)) to determine at which shear stress $\eta\dot{\gamma}$ a perfect fibre would break for a given length.

It was also observed that fibres were breaking-up even when the angle θ between them and the z' axis is smaller than $\pi/2$ (fibre out of the shear plan, see Fig. 2). Moreover, fibres spend a long time along the flow direction during a Jeffery rotation period, and the angle θ at this moment is maximal. Consequently, the angle between most of the fibres and the z' axis is almost all the time close to $\pi/2$. Therefore, the parameter θ was set to $\pi/2$ in the computations, supposing that even if some of the fibres were slightly out of the plan, they would also break-up.

3. Modelling approach

In order to turn these theoretical models in a computational method, specific tools, such as the probability distribution and the fragmentation matrix have to be used.

3.1. Probability distribution

Because the minimal radius of curvature is located in the middle of a bending fibre (Eq. (1)), a perfect fibre will always break-up at this point. However, a real fibre always presents defects which can be considered as weak points, leading to a possible break-up below the critical stress value. Therefore, introducing a statistical distribution of the breakage probability along the fibre was necessary in order to mimic the presence of defects. The usual breakage probability law for glass fibre reinforcement is the Weibull distribution [16]:

$$P(\sigma) = 1 - \exp\left[-\left(\frac{\sigma - \sigma_u}{\sigma_0}\right)^m\right] \tag{25}$$

where σ is the stress, σ_u the minimal stress for breakage, σ_0 a scale factor, and m a shape parameter. It expresses the probability for a fibre to break at the stress σ. The problem is that this law is only valid for a homogenous stress along the fibre, i.e. for a fibre loaded in tension. Consequently, the breakage probability (Eq. (25)) and the local breakage probability distribution along a fibre (Eq. (26)) were assumed to be uncorrelated.

The fibre breakage probability is (Fig. 5):

$$P(Bu) = \frac{1 - \exp(-Bu)}{1 - \exp(-1)} \quad \text{if } Bu < 1 \tag{25a}$$

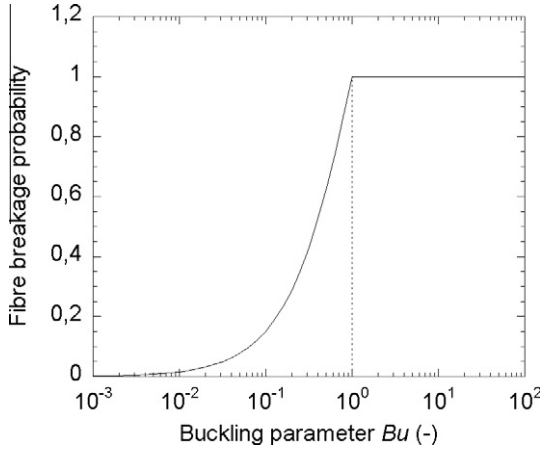

Fig. 5. Fibre breakage probability as function of buckling parameter *Bu*.

$$P(Bu) = 1 \quad \text{if } Bu > 1 \tag{25b}$$

This probability law allows a fibre to break below the buckling threshold because of the defects. The fibre necessarily breaks-up once this value is reached, complying with the previous theoretical observations (Fig. 3).

The local breakage probability distribution along the fibre was chosen as a Weibull-like distribution (Eq. (26)), but it remains possible to choose another type of distribution, for example a normal distribution [5].

The local breakage probability distribution on the fibre is (Fig. 6):

$$P_l(x) = \frac{1 - \exp\left[-\left(1 - \left(\frac{x}{a}\right)^2\right)^m\right]}{\int_{-1}^{1}\left(1 - \exp\left[-\left(1 - \left(\frac{x}{a}\right)^2\right)^m\right]\right)d\left(\frac{x}{a}\right)} \tag{26}$$

where m allows to change the distribution shape. The breakage probability is maximal at the middle of the fibre ($x = 0$). In this first approach, Weibull exponent m was set to 3, which is larger than any experimentally fitted value found in the literature. Doing so, a low enough "breakage polydispersity" was introduced in the model to ensure dispersion around the fibre centre position failure. A lower value for m did not change significantly the time-dependent distribution, as shown by a parameter study on m, for representative twin-screw extrusion conditions (not presented in the paper). The value $m = 3$ should then be considered as a minimal value to ensure variability in breakage position along the fibre.

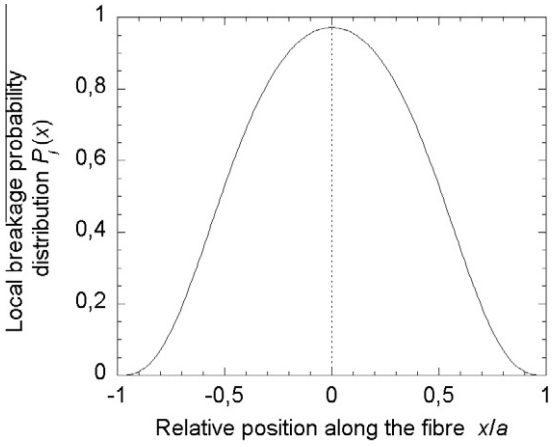

Fig. 6. Local breakage probability distribution along the fibre ($m = 3$).

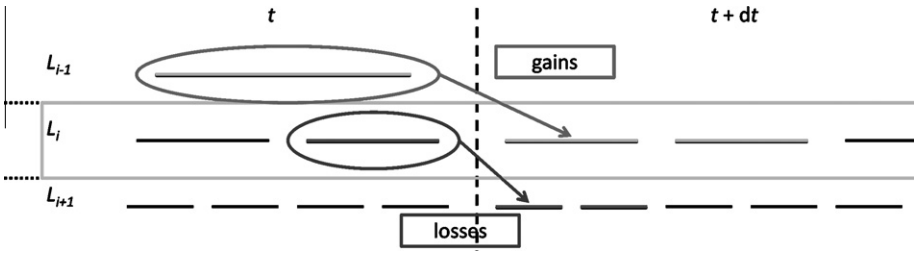

Fig. 7. Mass transfer from long fibre classes to shorter ones from the L_i length class point of view.

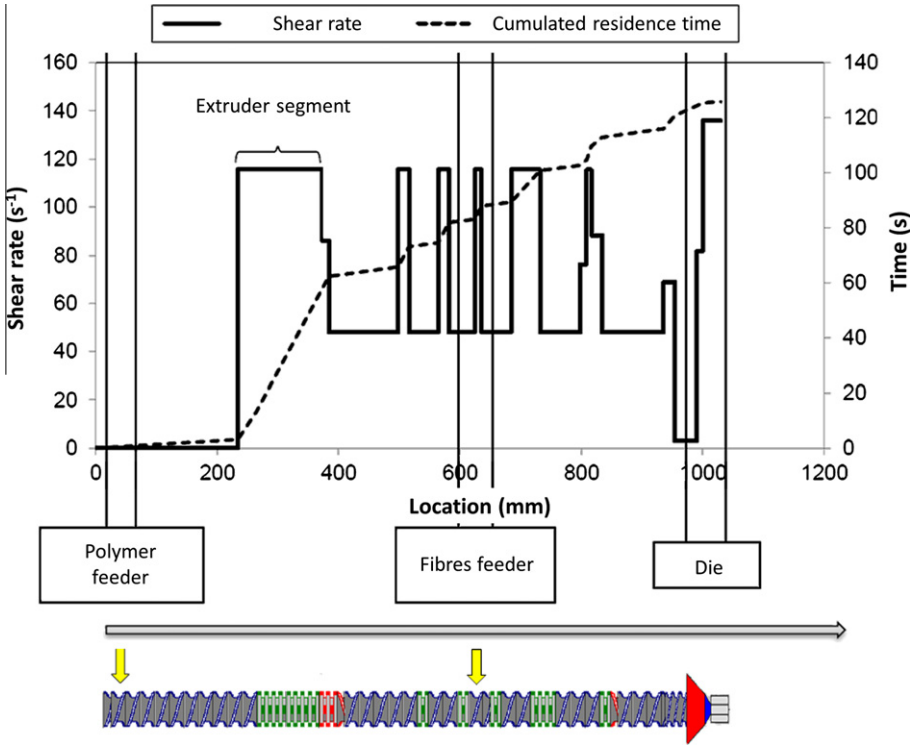

Fig. 8. Example of shear rate and cumulative residence-time along the twin-screw extruder computed using Ludovic® software. (For interpretation of the references to colour in this figure legend, the reader is referred to the web version of this article.)

3.2. Fragmentation matrix

In order to describe the entire distribution, a fragmentation matrix, based on the mass conservation [17] was used. Fibres were distributed into n classes according to their length. The minimal accessible length L_n was set to the minimal length below which a fibre cannot buckle for any applied stress ($\beta = 2.88$, Eq. (13)). Then, the mass transfer from long fibre classes to shorter ones (Fig. 7) was expressed using the set of Eq. (27), and solved with a Dormand–Prince method [18] using Matlab®.

The mass transfer set of equations is:

$$dm_i = \sum_{j=1}^{n} (\tau_j P_{ij} M_{ij}\, dt) - \tau_i m_i\, dt \quad \forall i,\ 1 < i < n \tag{27}$$

where m_i is the mass ratio represented by the fibres of length L_i, P_{ij} the probability for breaking-up a L_j length fibre to generate a L_i length one, M_{ij} (Eq. (28)) the mass transfer from the L_j length fibre class to the L_i length one (if a fibre breaks at the point required to generate a L_i length fibre), and τ_j the L_j length fibre breakage rate, that was considered to be equivalent with the L_j fibre length breakage probability per time unit. The quantities P_{ij}, M_{ij} and m_i are dimensionless and the breakage rate is expressed in s^{-1}. When a L_j length fibre breaks-up, generating a L_i length fibre, a part of its mass is transferred to the L_i length fibre class. The mass transfer between classes is then M_{ij}:

$$M_{ij} = \frac{L_i}{L_j} m_j \tag{28}$$

As the local breakage probability distribution on a fibre is symmetric relatively to its centre (Fig. 8), the probability P_{ij} for a breaking-up L_j length fibre to generate a L_i length one is twice the probability P_l (Eq. (26)) to break at one of the two possible points, leading to:

$$P_{ij} = 2P_l(x_i) \tag{29}$$

The L_j length fibre breakage rate τ_j was considered as equivalent to the probability for a L_j length fibre to break-up during a rotation period t_r divided by this period. The breakage probability P_{tr} during a period was computed by adding the breakage probabilities P (Eq. (25)) for each successive orientation $\mathbf{P}$ along the fibre orbit C:

$$P_{tr}(L_j) = \int_{orbitC} P(\sigma_B(\mathbf{P})) \frac{1}{Ct_r} dC \tag{30}$$

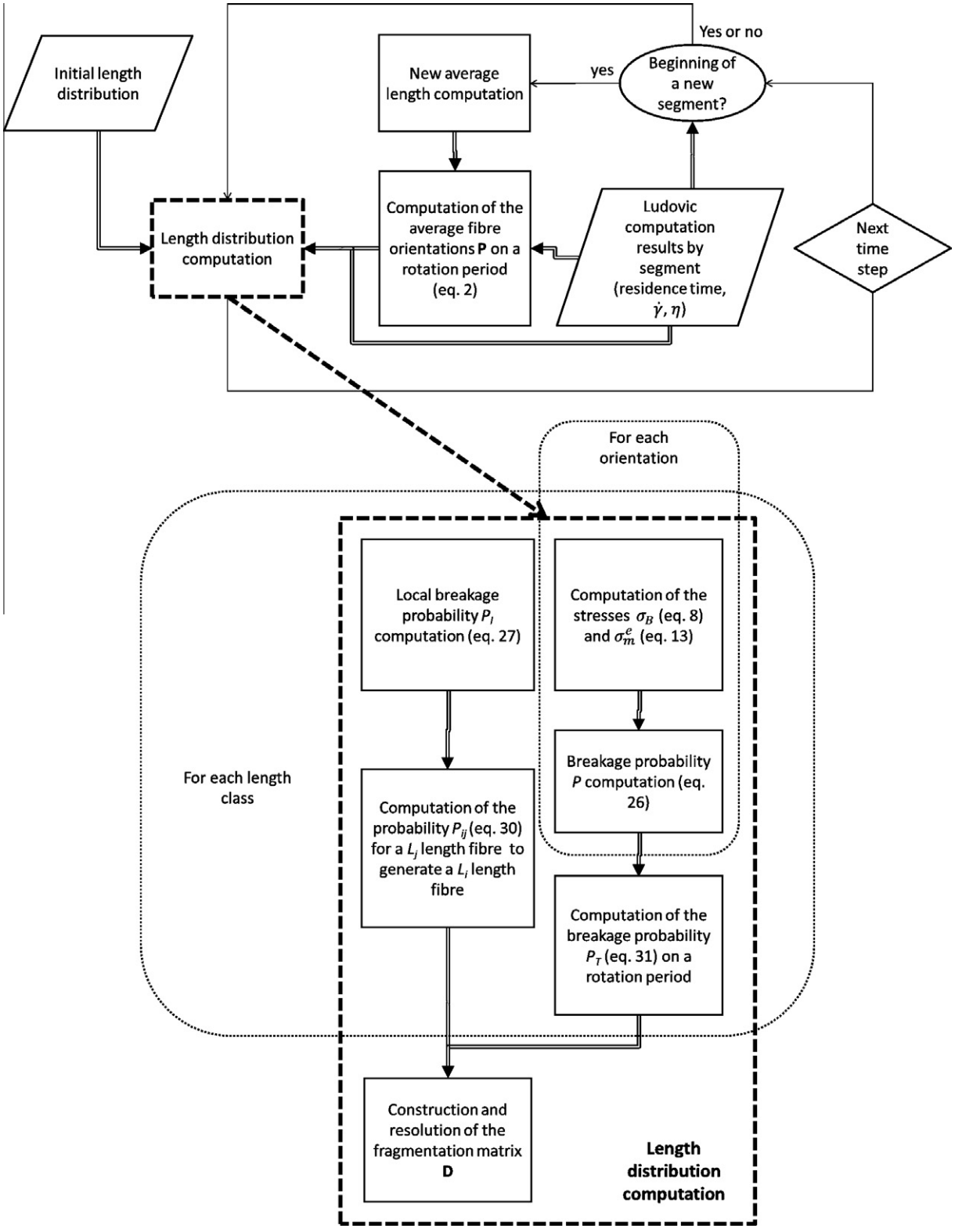

Fig. 9. Algorithm of the fibre break-up calculation.

where the stress σ_B (Eq. (7)) depends on the orientation **P** (or M), on the length L_j and on the shear rate $\dot{\gamma}$, C being the curvilinear abscissa on the orbit. The successive orientations **P** of a fibre during its rotation period are given by Jeffery equation (Eq. (2)). Jeffery period t_r^J is defined as:

$$t_r^J = \frac{2\pi}{\dot{\gamma}}\left(\beta_e + \frac{1}{\beta_e}\right) \tag{31}$$

In the case of constant strain rate, the Jeffery period scales the breakage rate in Eq. (32) and $t_r = t_r^J$. In the case of non constant strain rate, the rotation period t_r was computed numerically.

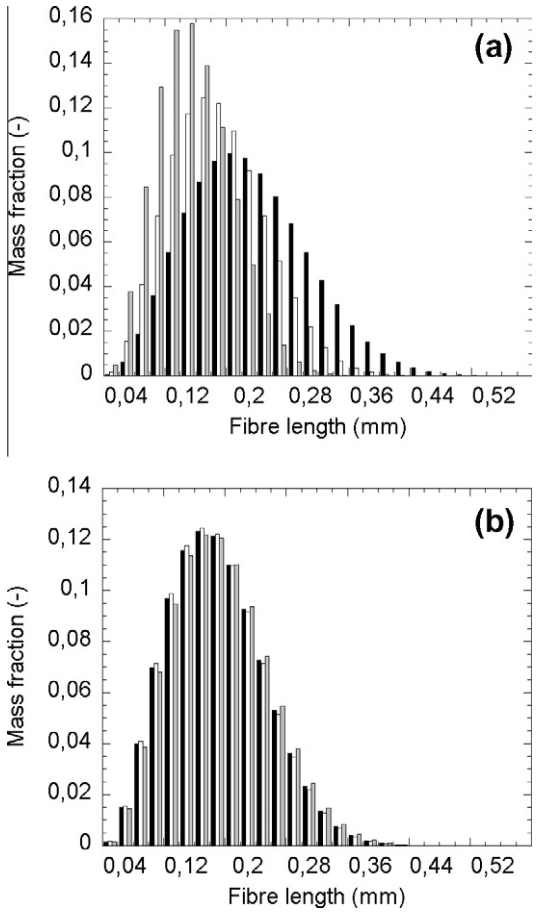

Fig. 10. Model sensitivity to parameters: final distribution after 10 s shearing for (a) different viscosities (■: 500 Pa s; □: 1000 Pa s; ▒: 2000 Pa s) for a constant shear rate ($\dot{\gamma} = 100\ s^{-1}$) or (b) different shear rates (■: 50 s^{-1}; □: 100 s^{-1}; ▒: 200 s^{-1}) for a constant shear stress (0.1 MPa, adjusting the viscosity).

From the probability P_{tr}, the breakage rate was obtained:

$$\tau_j = \frac{P_{tr}(L_j)}{t_r} \tag{32}$$

Input parameters for the simulation are the viscosity η, the shear rate $\dot{\gamma}$ and the residence time. Fibre characteristics, i.e. Young modulus (E = 72.4 GPa), initial length distribution and radius (b = 5 μm) are also needed. As explained previously, the angle θ was set to $\pi/2$.

3.3. Resolution algorithm

In order to calculate fibre breakage along a twin screw extruder, estimates of the shear rate and residence time in the various sections of the extruder must be computed. To do so, the Ludovic© software, developed in the laboratory and already largely used in different studies including fibre breakage [10,19–22], was used. The flow simulation with Ludovic© requires to define the screw profile, the polymer behaviour as well as processing conditions (feed rate, screw speed, and barrel temperature). The matrix viscosity was described by a Carreau–Yasuda law:

$$\eta(T) = \eta_0(T)[1 + (\lambda(T)\dot{\gamma})^a]^{\frac{n-1}{a}} \tag{33}$$

where η_0 is the zero-shear viscosity, λ a characteristic time, a the Yasuda parameter and n the power law index. η_0 and λ depend on temperature, according to Arrhenius laws:

$$\eta_0(T) = \eta_0 \exp\left[\frac{E_a}{R}\left(\frac{1}{T} - \frac{1}{T_0}\right)\right], \quad \lambda(T) = \lambda_0 \exp\left[\frac{E_a}{R}\left(\frac{1}{T} - \frac{1}{T_0}\right)\right] \tag{34}$$

where E_a is the activation energy, R the gas constant and η_0 and λ_0 reference values at the temperature T_0. Following values, corresponding to a polyamide, have been chosen: η_0 = 363 Pa s, λ_0 = 0.03 s, a = 1.01, n = 0.82, E_a = 54,000 J/mol, R = 8.34 J/K/mol, T_0 = 513 K. The polymer filled with 30 wt% glass fibres was also described by a Carreau–Yasuda law, with following values: η_0 = 4753 Pa s, λ_0 = 88.9 s, a = 3.7, n = 0.77. Parameters of the Arrhenius law were the same as for the unfilled matrix.

Computation starts from an experimental initial length distribution [10]. Then, flow conditions (shear rate, viscosity and residence time) along the twin-screw extruder were computed in a first step, using Ludovic® software (Fig. 8). Then, from the obtained data, the rotation of a fibre of average length was computed using Jeffery's equation (Eq. (2)). This "average" fibre was supposed to rotate in the shear plan (i.e. $\theta = \pi/2$). Afterwards, for each length class, the stress σ_B (Eq. (7)) applied on a fibre and the limit stress before buckling σ_m^e (Eq. (12)) were computed. The fibre breakage probability P (Eq. (25)) for each length class and for each obtained orientation was then calculated. Subsequently, the probability P_{tr} to break during a rotation period (Eq. (30)) was deduced for each length class. Then, for each length class, the local breakage probability distribution P_l along a fibre (Eq. (26)) was computed and the probability P_{ij} for a L_j length fibre to break-up generating a L_i length fibre (Eq. (29)) was deduced. Using all these values, the fragmentation matrix (Eq. (27)) was generated. Finally, the set of equations was solved with Matlab® and the obtained mass distribution was injected as the starting point for the next extruder segment computation. The global algorithm of fibre break-up calculation is shown Fig. 9.

This algorithm has been tested with different sets of parameters in order to study its sensitivity. The shear rate was used at two points of the simulation: the rotation computation and the shear stress computation. The obtained length distributions were found to be sensitive to the shear stress $\eta\dot{\gamma}$, but for a given shear stress, the distributions were not sensitive to the single shear rate $\dot{\gamma}$ (Fig. 10). It was concluded that in this simulation the shear rate was mostly acting on the fibres breakage through the shear stress. The final computed distribution was also found not to be very sensitive to the initial one. Thus, it was not necessary to use an accurately measured initial fibre length distribution to compute its evolution during a sufficiently long compounding process.

4. Examples of application

In order to validate the model, the evolution of fibre length distribution along a twin screw extruder was calculated and compared to experimental data previously obtained [13]. The experiments were carried out on a laboratory scale twin-screw extruder (ThermoFisher PTW 24) for different processing parameters (screw speed N from 200 to 600 rpm, feed rate Q from 5 to 9 kg/h). Dried polyamide 12 (PA12) (Rilsan A, kindly supplied by Arkema, France) was fed through the main feeder and mixed with 30 wt% glass fibres, added through a second feeder after PA12 melting. The initial average fibre length (in mass) was 3.48 mm and the fibre Young modulus was 72.4 GPa. Several samples were taken along the screws, after stopping the extruder and opening the clam-shell barrel. Fibre length measurements were achieved by optical microscopy and image analysis, after burning the samples and dispersing the recovered fibres into glycerol [10,11].

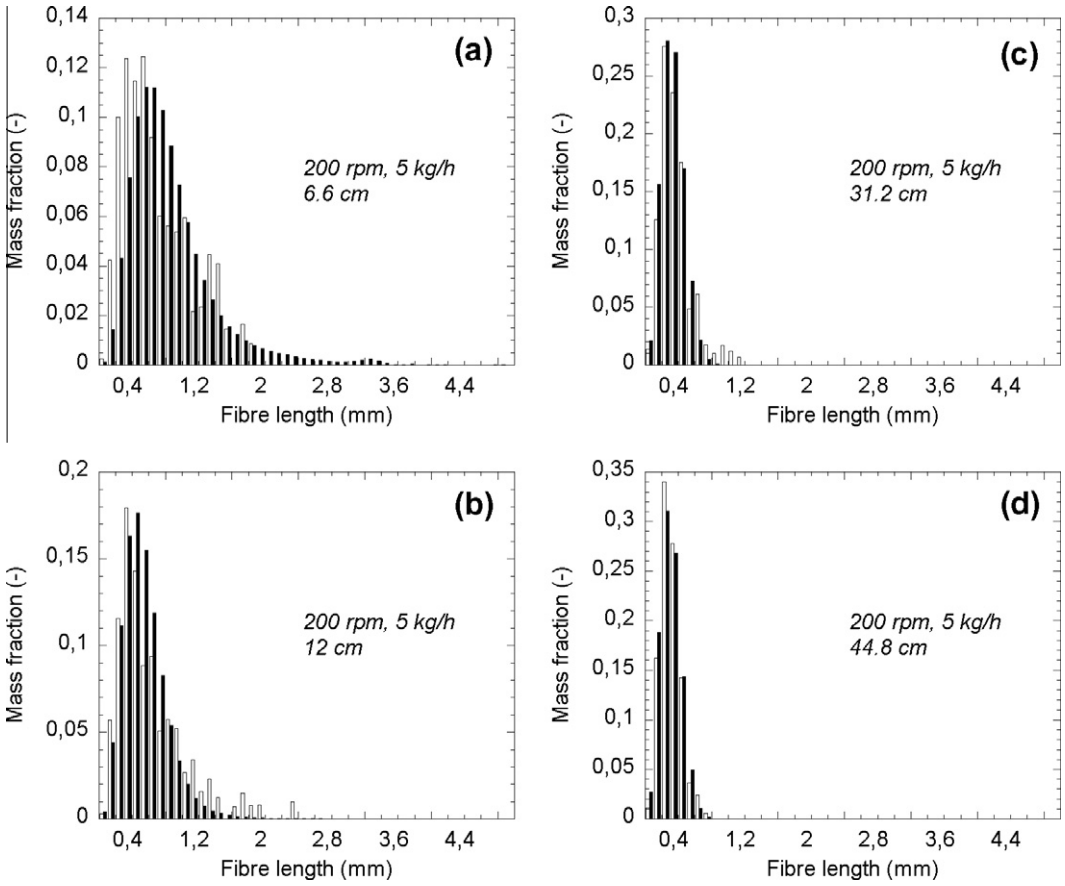

Fig. 11. Measured (white) and computed (black) length distributions. Screw rotation speed: 200 rpm, feed rate: 5 kg/h. Location from the fibres introduction: (a) 6.6 cm ± 0.5 cm, (b) 12 cm ± 0.5 cm, (c) 31.2 cm ± 0.5 cm, and (d) 44.8 cm ± 0.5 cm.

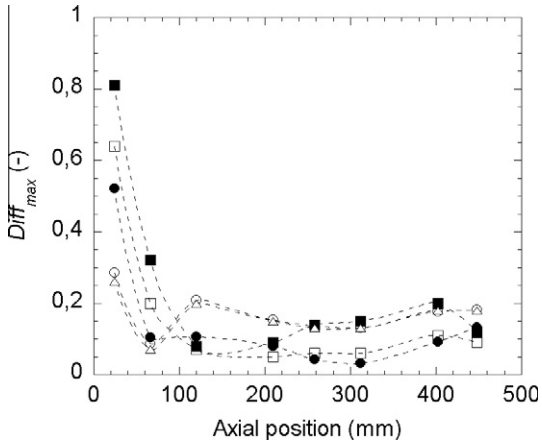

Fig. 12. Maximal difference between the experimental and the simulated cumulative distribution functions of the fibre length in number along the process for different process conditions (the dotted lines are just for guiding the eyes).

The computed fibre-length distributions were compared with the experimental ones at various locations along the screws, for five different sets of processing conditions. An example is shown in Fig. 11. Generally speaking, the shapes of the simulated fibre-length distributions corresponded quite well to the experimental ones. The effects of variation of the processing parameters were also correctly evaluated: a high rotation speed increased fibre breakage and a high feed rate limited it. Nevertheless, the experimental length distributions were very close from one set of parameters to another. Consequently, the accuracy of the model for different process conditions is not yet totally assessed.

The adequacy of the computed and measured length fibre distributions can be compared from one set of process parameters to another using the maximal difference between the experimental and the simulated cumulative distribution functions of the fibre length in number (Fig. 12):

$$Diff_{max} = \max_{L_n} |F_{exp}(L_n) - F_{sim}(L_n)| \tag{35}$$

$$\text{where} \quad F_{exp}(L_n) = \frac{\sum_{i=1}^{n} N_i}{\sum_{i=1}^{n_{tot}} N_i} \tag{36}$$

where N_i is the number of fibres of length L_i.

It appears that the beginning of the process was difficult to predict as the breakage rate was very high and consequently the error was larger. As the experimental samples have a certain thickness (a few mm), the error on the sampling position (and on the sampling time) could be important and might explain a part of the difference between experimental and calculated values.

Finally, the evolution of the average length in mass is shown on Fig. 13, as it is a common measure for fibre breakage study [9–11]. Once again, the agreement between model and experiments is satisfactory and was observed whatever the processing conditions (i.e. for different screw speeds and feed rates). However, it is a poorer representation of the fibre length evolution, as the length distribution might be sometime bi-modal.

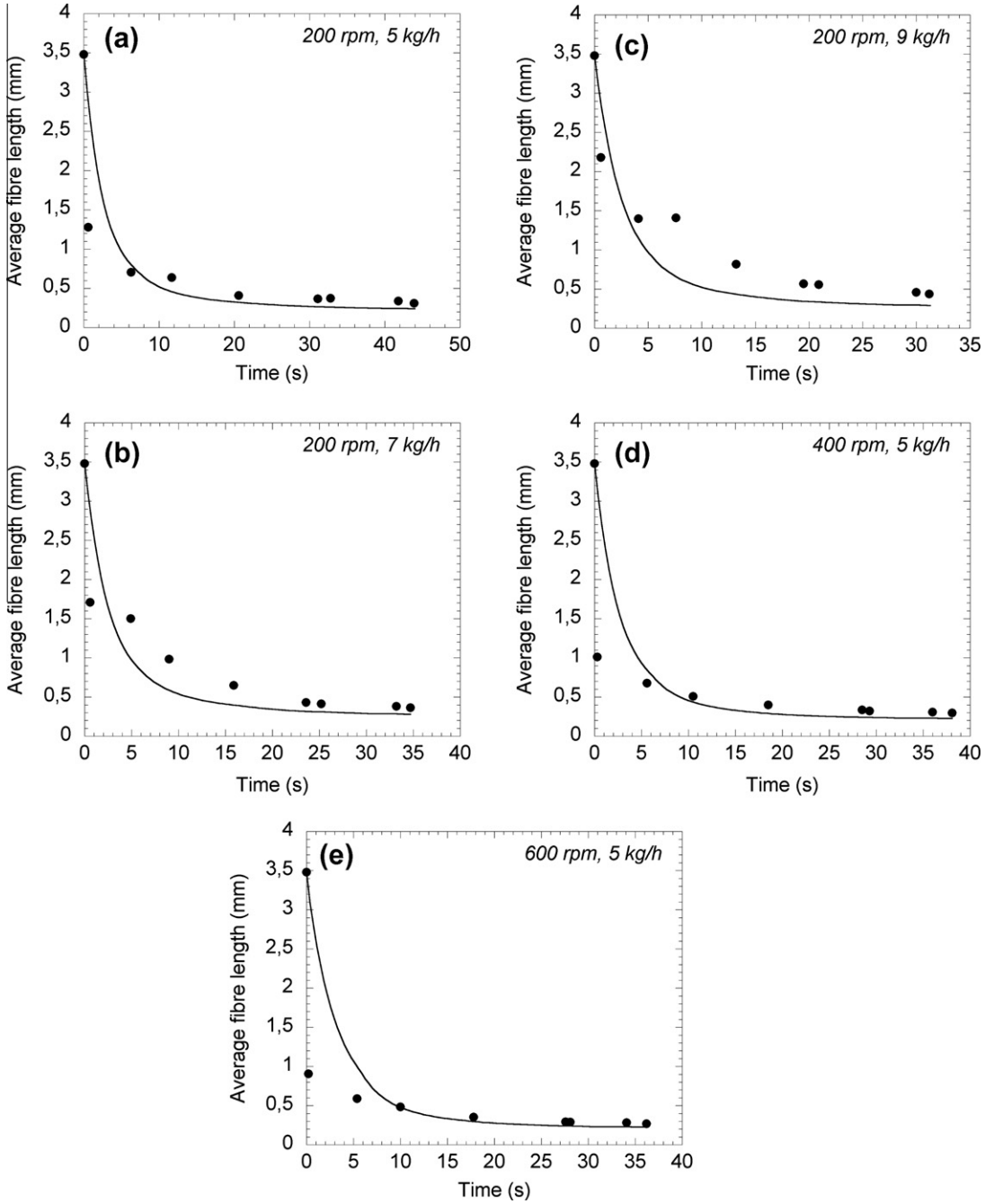

Fig. 13. Computed (full line) and measured (symbols) average lengths in mass. (a) Screw rotation speed: 200 rpm, feed rate: 5 kg/h. (b) Screw rotation speed: 200 rpm, feed rate: 7 kg/h. (c) Screw rotation speed: 200 rpm, feed rate: 9 kg/h. (d) Screw rotation speed: 400 rpm, feed rate: 5 kg/h. (e) Screw rotation speed: 600 rpm, feed rate: 5 kg/h.

5. Conclusion

A new computational method to predict changes in the fibre-length distribution during compounding in a twin-screw extruder was proposed. This evolution was calculated for five different sets of processing conditions, without adjusting any parameter, and these results were compared to experimental data. A satisfactory agreement was found, except at the early beginning of the process.

To summarise, this model, relying on a fragmentation matrix, seems to be able to predict fibre-length distribution in a twin-screw extrusion process quite accurately, but still needs to be validated more intensively.

Acknowledgments

This work was carried out in the context of the Fonlimics project, supported by FUI and labelled by the Plastipolis competitive cluster. We thank the DGE (Direction Générale des Entreprises, France) for its financial support.

References

[1] Vincent M, Devilers E, Agassant JF. Fiber orientation in injection molding of reinforced thermoplastics. J Non-Newt Fluid Mech 1997;73:317–26.
[2] Advani SG, Tucker III CL. The use tensor to describe and predict fiber orientation in short fiber composites. J Rheol 1987;31:751–84.

[3] Folgar F, Tucker III CL. Orientation behavior of fibers in concentrated suspensions. J Reinf Plast Compos 1984;3:98–119.
[4] Phelps JH, Tucker III CL. An anisotropic rotary diffusion model for fiber orientation in short- and long-fiber thermoplastics. J Non-Newt Fluid Mech 2009;156:165–76.
[5] Tucker III CL, Phelps JH, Abd El-Rahman AI, Kunc V, Frame BJ. Modeling fiber length attrition in molded long-fiber composites. In: Proceedings of PPS-26 Annual Meeting, Banff, July 2010.
[6] Wall D. The processing of fiber reinforced thermoplastics using co-rotating twin screw extruders. Polym Compos 1989;10:102.
[7] Shon K, White JL. A comparative study of fiber breakage in compounding glass fiber-reinforced thermoplastics in a buss kneader, modular co-rotating and counter-rotating twin screw extruders. Polym Eng Sci 1999;39:1757–68.
[8] Yilmazer U, Cansever M. Effects of processing conditions on the fiber length distribution and mechanical properties of glass fiber reinforced nylon 6. Polym Compos 2002;23:61–71.
[9] Shon K, Liu D, White JL. Experimental studies and modelling of development of dispersion and fiber damage in continuous compounding. Int Polym Proc 2005;20:322–31.
[10] Inceoglu F, Ville J, Ghamri N, Pradel JL, Durin A, Valette R, et al. Correlation between processing conditions and fiber breakage during compounding of glass fiber-reinforced polyamide. Polym Compos 2011;32:1842–50.
[11] Ville J, Inceoglu F, Ghamri N, Pradel JL, Durin A, Valette R, et al. A study of fiber breakage during compounding in a Buss kneader. Int Polym Proc 2012;27:245–51.
[12] Forgacs OL, Mason SG. Particle motions in sheared suspensions IX: spin and deformation of threadlike particles. J Colloid Sci 1959;14:457–72.
[13] Jeffery GB. The motion of ellipsoidal particles immersed in a viscous fluid. Proc R Soc A 1922;102:161–79.
[14] Burgers JM. On the motion of small particles of elongated form, suspended in a viscous liquid. In: Second report on viscosity and plasticity. New York: Nordemann Publishing; 1938.
[15] Massonet C, Cescotto S. Mécanique des Matériaux. Paris: De Boeck & Larcier; 1992.
[16] Weibull W. A statistical distribution function of wide applicability. J Appl Mech 1951;18:293–7.
[17] Blazy P, Yvon J, Jdid EA. Fragmentation appliquée aux minerais métalliques. Paris: Techniques de l'Ingénieur, JB3, J3050, 2006.
[18] Dormand JR, Prince PJ. A family of embedded Runge–Kutta formulae. J Comput Appl Math 1980;6:19–26.
[19] Vergnes B, Della Valle G, Delamare L. A global computer software for polymer flows in co-rotating twin screw extruders. Polym Eng Sci 1998;38:1781–92.
[20] Berzin F, Tara A, Tighzert L, Vergnes B. Importance of coupling between specific energy and viscosity in the modeling of twin screw extrusion of starchy products. Polym Eng Sci 2010;50:1758–66.
[21] Lertwimolnun W, Vergnes B. Influence of screw profile and extrusion conditions on the microstructure of polypropylene/organoclay nanocomposites. Polym Eng Sci 2007;47:2100–9.
[22] Berzin F, Tara A, Tighzert L, Vergnes B. Computation of starch cationization performances by twin screw extrusion. Polym Eng Sci 2007;47:112–9.